HHS Public Access

Author manuscript

J Am Chem Soc. Author manuscript; available in PMC 2020 June 03.

Published in final edited form as:

J Am Chem Soc. 2020 April 22; 142(16): 7514–7523. doi:10.1021/jacs.0c00590.

Structure and catalytic characterization of a second framework Al(IV) site in zeolite catalysts revealed by NMR at 35.2 Tesla

Kuzhi Chen[*,#], **Sarah Horstmeier**[◆], **Vy. T. Nguyen**[●], **Bin Wang**[●], **Steven Crossley**[●], **Tram Pham**[●], **Zhehong Gan**[#], **Ivan Hung**[#], **Jeffery L. White**[*,⊗], **School of Chemical Engineering, Oklahoma State University, Stillwater, OK 74078**

[#]National High Magnetic Field Laboratory, Tallahassee, FL

[◆]Department of Chemistry, Oklahoma State University, Stillwater, OK

[⊗]School of Chemical Engineering, Oklahoma State University, Stillwater, OK 74078

[●]School of Chemical, Materials, and Biological Engineering, University of Oklahoma, Norman, OK 73019

Abstract

Ultra-high field ^{27}Al{^{1}H} 2D correlation NMR experiments demonstrate that at least two framework Al(IV) sites with hydroxyl groups can exist in acidic zeolite catalysts in their dehydrated and catalytically active states. In addition to the known Al(IV) at the framework bridging acid site (BAS), a new site created by a second tetrahedral Al atom and its hydroxyl group protons in zeolite HZSM-5 are clearly resolved at 35.2 T field strengths, enabled by recently developed series-connected hybrid (SCH) magnet technology. Coupled with computational modeling, extensive ^{27}Al MQMAS experiments at multiple field strengths, and ^{1}H MAS NMR experiments, these data indicate that this second tetrahedrally-coordinated Al site (denoted Al(IV)-2) experiences an increased chemical shift and unique quadrupolar parameters relative to the BAS in both dehydrated and hydrated states. These new experimental data, supported by computational and catalytic reaction work, indicates that the second site arises from partially-bonded framework $(SiO)_{4-n}$-$Al(OH)_n$ species that significantly increase catalyst reactivity in benzene hydride-transfer and n-hexane cracking reactions. Al(IV)-2 sites result either from framework crystallization defects or from incomplete post-synthetic hydrolysis of a framework Al, prior to the formation of extraframework Al. Populations of this second acidic proton site created by the Al(IV)-2 species are shown to be controlled via post-synthetic catalyst treatments, should be general to different catalyst structures, and significantly enhance catalyst reactivity in the cited probe reactions when they are present. The results herein communicate the highest magnetic field strength data on active zeolite catalyst structures to date and enable for the first time the detection of Al and H association on a dry HZSM-5 catalyst, i.e., under conditions representative of typical end-use processes.

[*]Authors to whom all correspondence should be addressed at jeff.white@okstate.edu; kuzhi.chen@magnet.fsu.edu.

Supporting Information. Extensive additional information including experimental methods and their supporting references; details of fittings, simulations, and calculations; results from DFT calculations; ^{1}H and ^{29}Si solid-state NMR spectra; and static ^{27}Al 1D and MQMAS spectraHHH are provided and available free of charge via the Internet at http://pubs.acs.org.

Graphical Abstract

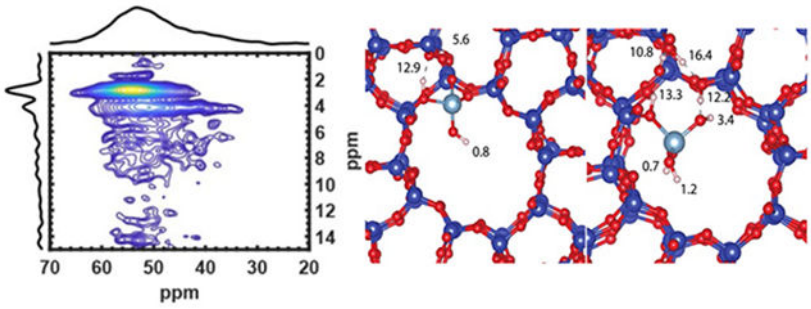

Introduction

Defining the structure of an active site and its possible structural variations is a critical step in developing fundamental insights into catalyst function, and exploiting those insights for improved catalytic materials.[1,2] Acidic zeolite catalysts have been successfully employed in several industrial processes,[3–5] most of which involve high-temperature conditions where water vapor or liquid water are absent. However, a growing interest exists in understanding the fate of zeolite acid sites in the presence of water, e.g., in catalytic transformation of feedstocks derived from alcohols and biomass,[6,7] which also requires accurate characterization of acid site structures both in the absence and presence of water. Tetrahedrally-coordinated framework Al atoms in zeolites create Brønsted acid sites through the charge-balancing function of a proton, and while it is known that crystallographically inequivalent framework Al sites can exist, e.g. 12 sites in the MFI family of zeolites of which HZSM-5 catalysts are a member, reports have demonstrated that the resulting bridging acid sites (BAS) in the different zeolite catalyst types are essentially identical in their ability to transfer a proton.[3] The MFI family of zeolite catalysts, most notably ZSM-5, are important to practical catalysis due to their efficacy in isomerization, alkylation, and disproportion reactions,[4,5,8] as well as in the conversion of methanol to hydrocarbons.[9,10] Currently, there is significant activity in the literature devoted to determining if single active sites, multiple sites, or a distribution of active acid sites exist in this commercially and academically important catalyst.[11–15] Recent reports suggest that proximity of the BAS's with each other, and with extra-framework hydroxyl groups, leads to acid site heterogeneity in many HZSM-5 catalysts, particularly at high Al content.[16–20] Here, the recently developed series-connected hybrid (SCH) magnet at 35.2 T[21] is coupled with two-dimensional $^{27}Al\{^{1}H\}$ correlation techniques[22–24] to conclusively identify a second Al(IV) species and accompanying Brønsted proton site in dry HZSM-5 catalysts. This second site in HZSM-5, while structurally unique compared to its known BAS, is also characterized by four-coordinate Al and denoted here as Al(IV)-2. Detailed experiments and supporting computational investigations on both dry and partially-hydrated HZSM-5 indicate that Al(IV)-2 is associated with a partially-bonded framework species that generates a Brønsted site, and similarly responds to post-synthetic treatments including solvent washing and hydrothermal exposure that have previously been used for modifying the distribution of extra-framework aluminum species. This new structure information is paramount to understanding the function of HZSM-5 catalysts in dry operating conditions, as well as

predicting the impact of water and other post-synthetic procedures on catalyst function, all of which are important to extending zeolite catalysts to increasingly complex feedstocks. We propose that the new acid site information reported here clarifies recent literature detailing the fact that catalysts with highest activity appear to have species other than isolated framework BAS's,[12–15] addresses uncertainties surrounding increased activity for some catalysts when exposed to small amounts of H_2O,[25–27] and provides key structural data for guiding the growing field of zeolite catalysis in water-rich processes.

Results

Dehydrated HZSM-5 catalysts were prepared in-house via the controlled deammoniation and dehydration of commercial NH_4^+ZSM-5 materials, resulting in one H^+ per framework Al site in the ideal limit. ^{27}Al solid-state NMR is routinely applied to characterize zeolite catalysts, albeit with difficulty in dehydrated catalysts due to large quadrupole coupling constant (C_q) associated with framework Al atoms in distorted symmetries following water removal.[28] At the lower magnetic fields commonly available, typically ca. 14 T and lower, framework signals are broadened beyond recognition due to the large second-order quadrupole coupling broadening, obscuring chemical shift information.[29,30] As such, the vast majority of data in the literature on HZSM-5 catalysts are for hydrated samples. Figure 1 shows ^{27}Al solid-state MAS (magic-angle spinning) NMR data on completely dehydrated HZSM-5 catalysts at relatively high and at ultra-high magnetic field strengths, i.e., 14, 19.6, and 35.2 T. As expected, Figure 1 shows that ultra-high field strength significantly narrows the line widths, allowing general recognition of Al bond orders. However, even at 35 T as shown in Figure 1, it is difficult to unequivocally resolve the features in the 50-60 ppm peak (1a). Aluminum atoms can exist in both framework and extra-framework sites,[31–33] and unequivocally associating Al sites with active Brønsted acid protons is not possible when only detecting Al, even when two-dimensional ^{27}Al multiple-quantum MAS (MQMAS) are used (*vide infra*). The key challenge is to understand the spatial and reactivity relationships between Al and H atoms in both the crystalline and non-crystalline regions of the catalyst in order to identify all potentially active Brønsted sites.

As general clarification to the reader less familiar with NMR of quadrupolar nuclei, it is important to note that the quadrupolar interaction arising from the coupling of the electric quadrupole moment in nuclei with spin quantum number > ½ to non-spherically symmetric electron distributions around the nucleus can dominate the lineshape in randomly-oriented powdered solids. This is the case for the ^{27}Al data discussed here, and even in spectra acquired under magic-angle spinning (MAS) conditions, higher-order quadrupolar interactions persist that dominate lineshapes at low magnetic field strengths, but become relatively less important at higher fields. For this reason, acquiring data at the highest field strengths possible is important for investigating ^{27}Al siting in catalysts, as reported here for data collected at 35.2 T, as well as comparing those data to data acquired at lower field strengths. For ^{27}Al spins in non-spherical bonding arrangements, e.g., trivalent, pentavalent, or distorted tetrahedral Al, the magnitude of the quadrupolar interaction (denoted as coupling constant C_q or interaction parameter P_q) is large and can reach several tens of MHz, obscuring chemical shift information, while those quadrupolar spins involved in tetrahedral or octahedral bonding exhibit reduced or vanishing quadrupolar interactions.

Figure 2 shows the $^{27}Al\{^{1}H\}$ Heteronuclear Multiple-Quantum Correlation (HMQC) NMR spectra for the same dehydrated HZSM-5 catalyst shown in Figure 1 acquired using the pulse sequence with dipolar recoupling or D-HMQC sequence.[22–24] Such a sequence has been recently used by Wang et. al. to characterize amorphous silica-alumina.[30] Figure 2a shows results obtained at 35.2 T (1500 MHz ^{1}H Larmor frequency), revealing that two distinct tetrahedral Al sites exist with apparent chemical shifts of 51 and 54 ppm, denoted Al(IV)-1 and Al(IV)-2, respectively. The HMQC data show for the first time that Al(IV)-1 and Al(IV)-2 are dipolar-coupled and spatially proximate to two chemically distinct protons at 4.2 and 2.8 ppm, respectively. Al(IV)-1 corresponds to an Al at the well-known BAS, based on extensive literature reporting known ^{27}Al and ^{1}H chemical shift values.[34,35] More important than their different apparent chemical shifts, examination of the linewidths of the extracted Al slices shown in the inset of 2a clearly shows that the two tetrahedral Al sites are distinctly different. Comparing Figure 2c to 2a shows that an order of magnitude increase in resolution for the ^{27}Al MAS dimension occurs when acquiring the HMQC data at 35.2 T relative to 14.1 T. More importantly, the presence of the 51/4.2 ppm and 54/2.8 ppm $^{27}Al/^{1}H$ couplings and their differing field-dependent slices clearly demonstrate that two tetrahedral Al sites exist which are coupled to two protons, thereby excluding a single-site Brønsted model for HZSM-5. For clarity and convenience to the reader, an expanded view of the 35.2 T contour plot in Figure 2a is provided in Figure S1. Most importantly, the 54/2.8 ppm $^{27}Al/^{1}H$ correlation result for the Al(IV)-2 site has implications for understanding catalysis in HZSM-5, as will be discussed in detail below.

Multiple-quantum magic-angle spinning (MQMAS) NMR can identify chemically unique Al atoms in materials.[36] Figure 3 shows variable-field strength ^{27}Al MQMAS spectra for the same dehydrated catalysts as shown in Figures 1 and 2, obtained at 35.2 and 19.6 T. Previously, Kentgens and coworkers have reported ^{27}Al MQMAS data on similar HZSM-5 catalysts at 14 T,[29] and our similar results at that field strength are not presented here for brevity. Figure 3 reveals two Al sites in the tetrahedaral region of the spectrum, whose isotropic chemical shifts δ_1 and δ_2 obtained after applying known methods for shearing and fitting of the second-order quadrupolar induced shifts δ_{qis} are 55 ppm and 59 ppm for the Al(IV)-1 and Al(IV)-2 sites, respectively.[37,38]

Due to the distribution of both the isotropic chemical shift values and of δ_{qis} values, the absolute values of the isotropic chemical shifts δ_1 and δ_2 are less critical than the fact that both shifts are in the known tetrahedral region. However, unlike the ultra-high field HMQC data in Figure 2, the data in Figure 3 cannot reveal if an Al atom in the catalyst generates a hydroxyl proton site. Table 1 summarizes key parameters obtained from fitting the multiple-magnetic field data in Figures 1–3, including both HMQC and MQMAS data, with additional details given in Figure S2–S5 and Table S1. Key outcomes are that the Al(IV)-2 species, which hosts the hydroxyl group giving rise to the 2.8 ppm ^{1}H signal, has an ^{27}Al isotropic shift that is clearly in the tetrahedral chemical shift region, and also exhibits a larger quadrupole asymmetry parameter but a smaller quadrupole coupling constant C_Q than the BAS Al(IV)-1 site. As a control, we note that the $\eta = 0.1$ for the Al(IV)-1 in the BAS agrees with previous reports,[29,46] and also with the calculated values from theory which are described along with computational support for other experimental results below.

Discussion

Many publications report that the most active forms of zeolite catalysts in general, and HZSM-5 in particular, contain more than just isolated crystalline BASs.[2,11,14,15,39,40] However, identification of structural moeties other than BASs that contribute to enhanced catalyst function is still a lively topic of debate, with multiple papers appearing in the current literature focusing on “synergistic” effects arising from nearest neighbor or proximate framework BASs,[18,39,41] Brønsted-Lewis synergies,[40,41] and Brønsted-Brønsted synergies.[19,44,45] The two latter categories include interactions between framework BASs and non-framework species. The general consensus is that the non-framework species are of the general structure $Al_x(OH)_y$, and free from the bonding constraints of the lattice, can migrate or block channels. The Al atom in EFAl (extra-framework aluminum) species is a Lewis acid, and many reports propose that EFAl species proximate to a BAS increases the reactivity of the latter via a Brønsted-Lewis synergy.[2,42,43] Hydrothermal treatments of zeolites increases the population of EFAl species through high-temperature water attack at Al tetrahedra in the lattice, which coincides with increased catalyst activity in high-temperature (ca. 500°C) probe reactions like cumene cracking as demonstrated many times for Y-type zeolites.[2,43] Other groups, particularly in the context of lower-temperature reactions, have shown that Brønsted-Brønsted synergies between BASs and non-framework aluminols increase catalyst activity,[19] with some computational reports even calling into question the existence of Brønsted-Lewis synergies altogether in some zeotypes.[44,45] NMR spectroscopy has played a key role in trying to understand structure and reactivity relationships in the context of catalyst synthesis and post-synthetic treatments, with the observation of Al (IV) signals in the known tetrahedral 50-65 ppm region vs. Al(VI) signals near 0 ppm as the most commonly employed marker of BAS framework Al and EFAl in HZSM-5 catalysts, respectively.[38,46,47] The limitations of detecting signals from quadrupolar Al atoms in non-spherical bonding environments are well known, which is why the majority of data in the literature centers on hydrated HZSM-5 catalysts. Similarly, signals at 4.0-4.5 and 2.5-2.9 ppm in ^{1}H solid-state NMR spectra of dehydrated HZSM-5 have been used as indicators of hydroxyl groups on BAS and EFAl species, respectively.[35,46] Thus, the presence of a 2.8 ppm signal in the proton spectrum or the proton dimension of a 2D heteronuclear correlation spectrum would indicate hydroxyl groups from EFAl species, based on historical literature assignments.

The dipolar HMQC data in Figure 2 shows that a tetrahedral Al atom with a signal at 51 ppm at 35.2 T is coupled to a ^{1}H whose signal appears at 4.2 ppm. This correlation arises from the framework BAS involving Al(IV)-1 and its bridging hydroxyl proton, as shown in Figure 4a, and is expected. The known values for the BAS serve as an important internal calibration. Conversely, the correlation between the 54 ppm Al(IV)-2 signal and the 2.8 ppm ^{1}H signal is not expected, since that ^{27}Al signal clearly arises from an aluminum atom in a tetrahedral bonding environment, and the literature assigns the 2.8 ppm ^{1}H signal to hydroxyls on EFAl species that are not tetrahedral Al(IV), but rather Al(III), Al(V), or Al(VI).[35,46] Recent literature indicates that the protons giving rise to the 2.8 ppm signal are themselves reactive, and when removed from the catalyst using known methods for zeolite EFAl extraction like ammonium hexafluorosilicate (AHFS) washing, overall reaction rates

decrease.[14,15,19,48] AHFS washing, under appropriate conditions, can selectively remove Al that is not associated with a framework BAS while leaving BASs intact, thereby generating a "clean" catalyst.[14,15,19] Previously, it has been shown that the 2.8 ppm signal for HZSM-5 catalysts can be completely removed by mild AHFS washing, and then re-introduced when the washed catalyst is subjected to wet flowing air at ca. 500°C, i.e., steaming.[40] Similarly, the MQMAS ^{27}Al spectra in Figure 5 demonstrate that the Al(IV)-2 signal behaves in an identical fashion, i.e., it is removed by mild AHFS washing (5a-b), and re-introduced by steaming (5c-e). In addition to the spectroscopic correlation of signals for the Al(IV)-2 species in the HMQC as seen via the 54/2.8 ppm cross ^{27}Al/^{1}H peaks, there is also a chemical correlation due to the fact that both signals respond in an identical fashion to post-synthetic AHFS treatments.

It is important to point out that the HMQC correlations between Al(IV)-2 and its ^{1}H signal do not mean that the only protons associated with Al(IV)-2 are weakly acidic, as suggested by the low ^{1}H chemical shift value of 2.8 ppm. The charge-balancing proton created by Al(IV)-2, shown in red in Figure 4, will likely exhibit a broad chemical shift range due to its complex hydrogen bonding environment. Figure S6 shows that the dry initial catalyst, prior to AHFS washing or any steaming, exhibits a broad signal from 12-15 ppm in addition to a broad 5-7 ppm signal. As previously shown,[14,19] these signals, along with the 2.8 ppm signal, are removed by AHFS washing. The 2.8 ppm and 12-15 ppm ^{1}H signals are detected together as long as the catalyst is sufficiently dry; trace moisture leads to chemical exchange for the acidic 12-15 ppm signal protons. Since the 12-15 ppm signal is weak, it is difficult to clearly resolve in the HMQC data of Figure 2. That the hydroxyl groups generating the 2.8 ppm and 12-15 ppm hydroxyl groups are simultaneously proximate is proven by the ^{1}H-^{1}H DQSQ data shown in Figure S7 for the dry HZSM-5 catalyst, in which their specific correlation is observed at the double-quantum frequency shown by the summed chemical shift at (2.8 ppm + 12.5 ppm) = 15.3 ppm in the selected slice. Similarly, the entire broad 12-15 ppm signal is correlated with the 2.8 ppm signal, giving a range in the double-quantum axis. In total, these data in concert with the DFT quadrupolar parameters in Figure 6 and chemical shift calculations in Figure S9–S11 (*vide infra*), are consistent with the proposed structures in Figure 4b–d.

The combined spectroscopic and post-synthetic catalyst treatment results indicate that the Al(IV)-2 species, and its ^{1}H-containing hydroxyl groups, are associated with the framework as partially-hydrolyzed but still partially-bonded Brønsted site of the types shown in Figures 4b – 4d. The Al(IV)-2 Brønsted protons are denoted by red in Figures 4b–d, and by definition they must exist if associated with a hydroxyl group on an Al(IV) atom due to charge balance requirements. Previously, Kentgens has assigned an Al(IV)-2 species in an HZSM-5 catalyst to framework BAS Al species perturbed by cations like Na^{+}, or to EFAl.[29] However, that does not agree with our HMQC correlation data in this case since Al(IV)-2 is correlated to Al-OH that is removed by AHFS, and created by steaming, as described above. It is important to recognize that both the Al(IV)-2 ^{27}Al signal and its associated ^{1}H signal are observed in the absence of a 0-ppm Al(VI) or a 30-40 ppm Al(V) signals in dehydrated catalysts. Figure S8 shows additional comparative data for Si/Al=11.5, including the full chemical shift range as a function of catalyst history that indicates Al(III) or Al(V) is never present in detectable amounts unless the catalyst is steamed.

Further evidence supporting the assignment of an active Brønsted site at partially-bonded Al(IV)-2 species comes from DFT calculations shown in Figure 6 with additional calculated structures in Figure S9–S11.[51,52] The absolute chemical shift tensor of Al in aluminium acetylacetonate $Al(acac)_3$ was calculated for a reference, yielding a value of −562 ppm. Using this as the reference, the chemical shift of Al in Fig. 6 can be converted to 59, 74 and 77 ppm for the intrinsic site, the one with one water incorporated, and the one with three water in the structure, respectively. The chemical shift of Al is very sensitive to the local distortion as shown in Figure S9; the chemical shift of the Al at the early stage of hydrolysis (one water incorporated) could range from 65 to 74 ppm, or an uncertainty in the chemical shift calculation on the order of 10 ppm. The chemical shift trends caused by partial hydrolysis agrees with the experimental results in Table 1 and Figures 2 and 3, though the calculated changes (6 – 15 ppm) are larger than the experimental value of 4 ppm.

Figure 6 shows calculated structures for two of the four species shown above in Figure 4, with chemical shift and shielding information, quadrupole coupling constant C_Q, and asymmetry parameter η_Q reported in the figure. While there can be deviations in absolute values of any of these parameters based on small changes in bond angles surrounding any Al center, the trends are in close agreement with the experimental data reported above. Comparing the BAS Al(IV)-1 in 6a with the Al species in 6b, for example, shows that the latter Al species in a partially-bonded framework position has reduced chemical shielding by ca. 12 ppm (i.e., larger chemical shift), a smaller C_Q, and a larger η_Q. Recall, the Al(IV)-2 experimental data summarized in Table 1 shows a larger chemical shift by 3-4 ppm, a smaller C_q by +6 MHz, and η_Q = 0.6 versus 0.1 for the BAS Al(IV)-1. Figure 6b shows the structure resulting from one water of addition at the BAS, and similar trends are observed after addition of three water molecules. The value of C_Q is very sensitive to local disorder. Conversely, as shown in Figure S10, ^{27}Al chemical shift and quadrupolar parameters for trivalent Al(III) species of the type commonly associated with extra-framework Al are completely inconsistent with the experimental data for the Al(IV)-2 species discussed above. Other Al(IV) configurations following addition of one water molecule are shown in Figure S9. In addition, Figure S11 shows the calculated results for ^{1}H chemical shifts, exhibiting the well-known isolated BAS signal near the experimental 4.2 ppm, as well as other shifts significantly downfield in the 11-16 ppm region which also agrees with recently reported experimental shifts in the 12-15 ppm region for HZSM-5.[14,19,40.]

Additional key evidence for the role of partially-bonded framework structures as the source of Al(IV)-2 comes from examination of ^{29}Si NMR of HZSM-5. Figure S12 shows that a small amount of Si with one adjacent Al(IV) is removed following AHFS treatment. However, previous publications show that BAS hydroxyl groups are not perturbed, which must occur if a BAS Al is extracted.[14,15] Those same publications show that signals traditionally assigned to EFAl OH's, i.e. the 2.8 ppm peak in the ^{1}H MAS NMR spectra, are attenuated or completely eliminated as recently reported.[14,15,19,40] Also, there is no apparent correlation between the presence of a 0-ppm Al(VI) peak in Al MAS NMR data and the 2.8 ppm peak in ^{1}H NMR data; strong 2.8 ppm peaks are routinely observed in the absence of a 0-ppm Al(VI) signal. All of these inconsistences are explained by a contribution from the structures in Figure 4 that are experimentally confirmed by the 35.2 T HMQC data in Figure 2 and the supporting analyses described herein. Such structures would be more susceptible

to attack by AHFS than framework BASs, similar to what has been observed for EFAl species. These same structures are predicted by computational analysis of partial hydrolysis products in zeolites subjected to dealumination steps, as reported recently, and would also be present from incomplete framework condensation during synthesis, particularly for the high-Al content zeolites discussed here.[49,50]

Al(IV)-2 Impact on Catalysis.

Table 2 summarizes the relationship between catalyst reactivity and the relative amounts of the traditional BAS arising from Al(IV)-1 and its associated bridging hydroxyl group versus that of Al(IV)-2 and its hydroxyl groups. This table should be viewed along with ^{1}H and ^{27}Al spectra in Figures S6 and S13, and recalling Figure 2 demonstrating the H-Al correlations. Pulsed microreactor conversions of n-hexane at 480°C was used to measure the activity of catalysts under very low conversion conditions, less than 12%, to emphasize primary reaction steps and limit secondary reactions, details for which have been previously described and also found in the SI.[19] No catalyst deactivation was observed. The product distribution, shown in Figure S14, is comparable with previously reported selectivity.[53] The activities of the catalysts do not depend in a straightforward way on the amount of total Brønsted acidity as measured by traditional IPA TPD. As shown in Table 2, the Si/Al = 11.5 catalyst has more BAS and total acidity than the 15 catalyst but exhibits less than half of the latter's conversion. Washing the Si/Al = 15 catalyst with AHFS under mild conditions does not significantly impact the total amount of Al(IV)-1 or its BAS proton concentration as shown in the third column of Table 2, but it does significantly reduce the Al(IV)-2 and its associated hydroxyl group, as shown in the fourth and fifth column. Catalysts prepared in this way have the lowest conversion for n-hexane, and also the lowest H/D exchange rate constant in room temperature reactions with benzene-d_6 as shown in the last two columns. Again, the data shown in Figures 3, 5, S6, and S13 clearly indicate that reactivity depends on variations in the new Al(IV)-2 species discussed here, and not detectable variations in Al(III), Al(V), and Al(VI) species. While such variations may exist, the magnitude of the original amount of Al(IV)-2 and its changes with catalyst selection or post-treatment are much larger than any of the aforementioned species, and also larger than any changes in Al(IV)-1 and its BAS proton concentration, and therefore cannot be ignored.

Summary of evidence for Al(IV)-2 identification and structure assignment.

Al(IV)-2 cannot be assigned to traditional EFAl species, i.e., Al(III), Al(V), or Al(VI) for the following reasons. Firstly, the second type of Al(IV) described here is an Al atom that is tetrahedrally bonded to four oxygen atoms, based on known chemical shift and C_q data, thus possessing a negative formal charge. Al(IV)-2 cannot be a Lewis acid, since it has a negative formal charge. Dimers or trimers of a non-framework $Al(OH)_4^-$ would also be negatively charged, and thus unable to function as a Lewis acid. Secondly, due to the requisite Al(IV) charge, a proton associated with it is required as indicated in Figure 4. Figures 2, S6, and S13 show that the Al(IV)-2 species and its hydroxyl group are the key varying structural moiety in these catalysts based on preparation and post-synthetic treatments. Figures S9 and S10 demonstrate that the quadrupolar parameters for Al(IV)-2 are significantly different than those for Al(III) species. Finally, the new Al(IV)-2 reported here is bonded to a Si atom, as shown by the data in Figure S12, which shows it is associated with the framework and

cannot be assigned to extraframework species. Most importantly, as shown in Figures 3a and 3b, Al(IV)-2 is detected prior to any extraframework Al(V) or Al(VI) species in the dry catalysts, the latter of which give rise to the known ca. 30 ppm and 0 ppm signals that are typically used as evidence for dealumination. No signals are observed at 0 or 30 ppm in Figure 3 for the dry catalysts. The structure and chemical relevance of tetrahedrally-coordinated Al(IV)-2 cannot be attributed to EFAl, and exists in the absence of detectable ^{27}Al signals arising from EFAl, as shown for the unsteamed and untreated NH4ZSM-5 sample in Figure S15.

To our knowledge, partially bonded Al(IV) has been previously proposed based on theory,[49] but without experimental evidence showing that it can be an active species in zeolites. The experimental data presented here shows direct evidence for their existence and catalytic relevance. Previous works by Prins and Bokhoven discussing partially dislodged Al referred to octahedral aluminum, and involved either Beta or Y-type zeolites.[55–57] From that work, it appears that only Al(VI) can be re-inserted to the framework by NH_3 treatment, not Al(IV). In recent work, framework-associated Al(VI) Lewis sites were reported in mordenite, or as dislodged Al(IV) that was hydrated.[54,56] The previous MQMAS work by Kentgens describing a second Al(IV) site in MFI likely detected the same species reported as Al(IV)-2 in our MQMAS data, albeit without the structural insight afforded by the HMQC and other solid-state NMR data reported here for dry catalysts.[29] The structures discussed in previous contributions are not the same as the Al(IV)-2 species proposed here, as Figure S12 indicates that Al(IV)-2 is chemically bonded to Si atoms. For the MFI samples used in our work, it is reasonable that partially-bonded Al(IV)-2 forms before extra-framework Al species form. As can be seen in the attached full chemical shift range ^{27}Al MQMAS Figure S8, Al(V) can of course be formed and detected after severe hydrothermal treatment, but Al(IV)-2 is logically formed earlier than Al(V).

Summary of Al sites in hydrated vs. dehydrated catalysts.

The data show that Al(IV)-2 has the higher chemical shift and smaller P_q relative to Al(IV)-1 in the dehydrated catalysts, but a larger P_q and apparent lower chemical shift in the hydrated catalysts. Upon hydration, it is known the Al(IV)-1 site is surrounded by clusters of water molecules that delocalize the H^+ charge through rapid chemical exchange, and since that Al is bonded to four Si atoms via oxygen bridges, near-tetrahedral geometry results in a negligible electric field gradient and detectable Al NMR spectra under normal acquisition conditions. Conversely, when water is removed from Al(IV)-1, the localized charge and concomitant lattice strain resulting from bonding to fixed framework Si-O moieties is significant, leading to large P_q values of the magnitude shown in Table 1. In all cases, Al(IV)-1 is bonded via oxygen bridges to four framework Si atoms, and thus the 55-ppm isotropic chemical shift does not change significantly as a function of hydration. Al(IV)-2, by virtue of the fact that it is bonded to both framework SiO moieties and hydroxyl groups as in Figures 6b and 6c, maintains a significant electric-field gradient upon hydration due to interactions between the hydroxyl groups and water molecules. An apparent lower chemical shift for Al(IV)-2 relative to Al(IV)-1 in the hydrated case shown in Figure 5 results from the large δ_{qis} for the former. D-HMQC experiments of the type shown in Figure 2 for the dehydrated cases are not reliable for fully-hydrated catalyst samples due rapid proton

chemical exchange which is well-known to occur; such experiments will emphasize only the most rigid Al-H pairs.

Relevance of Al(IV)-2 to location, topology, and proximity contributions to catalyst reactivity.

Contributions from Iglesia, Bell, and Lercher, among others, have recently shown that catalyst activity can depend on several factors, including active site location,[12,15] channel structures and their chemical composition,[58–62] and proximity to EFAl species.[63] Very recent work by Lercher's group suggests that creating BASs with proximate EFAl species contributes more significantly to increased catalyst activity.[64] In each of these works where proximate EFAl effects contribute, strong and intense signals in the Al NMR at either 0- or ca. 30-ppm are observed following specific steaming protocols. It is important to note that in our work, only Al(IV)-1 and Al(IV)-2 signals are observed in the 50-60 ppm region of the spectrum in catalysts that have not been steamed; EFAl signals are not observed as can be seen in Figure 3 on dry HZSM-5 prior to any treatments, even at the highest 35.2 T field strength shown by 3a. Also, the lack of any EFAl signals but significant Al(IV)-2 signal is shown in Figure S15, which was obtained on an unexchanged NH_4^+ZSM5 sample. Unsteamed and untreated catalysts that have both Al(IV)-1 and Al(IV)-2 sites, with their associated hydroxyl groups, are more active in the cracking and H/D exchange reactions discussed above than catalysts that have only the traditional isolated BAS created by Al(IV)-1, as shown by the data in Table 2. These results in no way preclude any of the enhancements afforded by EFAl species once they are formed, as discussed in the references cited immediately above. Rather, they afford additional atomistic detail of framework contributions to reactivity that are more complex than can be attributed to a single type of framework acid site, and further must be considered when trying to fully predict the impact of synergistic EFAl effects since Al(IV)-2 sites can ultimately generate EFAl species after steaming.

Conclusions

In summary, the ultra-high magnetic field data and supporting computational data reveals that zeolites can have at least two types of chemically-distinct tetrahedral aluminum atoms associated with the zeolite framework, thereby creating the possibility for two chemically-distinct Brønsted sites. The room-temperature H/D exchange experiments and the high-temperature n-hexane creacking experiments indicate that Al(IV)-2 and its accompanying hydroxyl groups increase catalyst activity relative to catalysts that only contain Al(IV)-1 and its associated BAS. The observed results cannot be easily attributed to Al atoms in non-framework species, as the latter were in most cases not detected, or detected in trace amounts well below that of the partially-coordinated Al(IV)-2 sites. The data suggest that the collective understanding and practical implementation of zeolite-based catalysis can include synthetic and post-synthetic modification to target these partially-coordinated framework Al(IV) sites, potentially leading to increased catalytic activity and longevity through the strategic use of water, as will be explored in future work.

Supplementary Material

Refer to Web version on PubMed Central for supplementary material.

Acknowledgements.

This material is based upon work supported by the National Science Foundation under Grant Nos. CHE-1764116 and CHE-1764130, and are gratefully acknowledged. Partial instrumentation support for the solid-state NMR system at Oklahoma State University was provided in part through the Oklahoma State University Core Facilities program. Development of the SCH magnet and NMR instrumentation was supported by NSF (DMR-1039938 and DMR-0603042). The operations of the SCH magnet and the NMR Spectroscopy operations are overseen respectively by the DC User Facility and the NMR and MRI User Facility at the NHMFL that is supported by NSF DMR-1157490 and the State of Florida. The user activities of the SCH are further supported by NIH P41 GM122698.

References

1. Trickett CA; Osborn Popp TM; Su J; Yan C; Weisberg J; Huq A; Urban P; Jiang J; Kalmutzki MJ; Liu Q; Baek J; Head-Gordon MP; Somorjai GA; Reimer JA; Yaghi OM, Identification of the strong Brønsted acid site in a metal–organic framework solid acid catalyst. Nature Chemistry 2019, 11 (2), 170–176.
2. Haag WO; Lago RM; Weisz PB, The active site of acidic aluminosilicate catalysts. Nature 1984, 309, 589.
3. Xu B; Sievers C; Hong SB; Prins R; van Bokhoven JA, Catalytic activity of Brønsted acid sites in zeolites: Intrinsic activity, rate-limiting step, and influence of the local structure of the acid sites. J. Catal 2006, 244 (2), 163–168.
4. Kissin YV, Chemical Mechanisms of Catalytic Cracking Over Solid Acidic Catalyst: Alkanes and Alkenes. Catalysis Reviews 2001, 43 (1-2), 85–146.
5. Corma A, Inorganic Solid Acids and Their Use in Acid-Catalyzed Hydrocarbon Reactions. Chem. Rev 1995, 95 (3), 559–614.
6. Ennaert T; Van Aelst J; Dijkmans J; De Clercq R; Schutyser W; Dusselier M; Verboekend D; Sels BF, Potential and challenges of zeolite chemistry in the catalytic conversion of biomass. Chem. Soc. Rev 2016, 45 (3), 584–611. [PubMed: 26691750]
7. Zapata PA; Faria J; Ruiz MP; Jentoft RE; Resasco DE, Hydrophobic Zeolites for Biofuel Upgrading Reactions at the Liquid–Liquid Interface in Water/Oil Emulsions. J. Am. Chem. Soc 2012, 134 (20), 8570–8578. [PubMed: 22548687]
8. Corma A; Orchillés AV, Current Views on the Mechanism of Catalytic Cracking. Microporous Mesoporous Mater. 2000, 35-36, 21–30.
9. Tian P; Wei Y; Ye M; Liu Z, Methanol to Olefins (MTO): From Fundamentals to Commercialization. ACS Catalysis 2015, 5 (3), 1922–1938.
10. Ilias S; Bhan A, Mechanism of the Catalytic Conversion of Methanol to Hydrocarbons. ACS Catalysis 2013, 3 (1), 18–31.
11. Knott BC; Nimlos CT; Robichaud DJ; Nimlos MR; Kim S; Gounder R, Consideration of the Aluminum Distribution in Zeolites in Theoretical and Experimental Catalysis Research. ACS Catalysis 2018, 8 (2), 770–784.
12. Jones AJ; Carr RT; Zones SI; Iglesia E, Acid strength and solvation in catalysis by MFI zeolites and effects of the identity, concentration and location of framework heteroatoms. J. Catal 2014, 312 (0), 58–68.
13. Pashkova V; Sklenak S; Klein P; Urbanova M; Dědeček J, Location of Framework Al Atoms in the Channels of ZSM-5: Effect of the (Hydrothermal) Synthesis. Chemistry, A European Journal 2016, 22 (12), 3937–3941.
14. Chen K; Abdolrhamani M; Sheets E; Freeman J; Ward G; White JL, Direct Detection of Multiple Acidic Proton Sites in Zeolite HZSM-5. J. Am. Chem. Soc 2017, 139 (51), 18698–18704. [PubMed: 29211463]

15. Schallmoser S; Ikuno T; Wagenhofer MF; Kolvenbach R; Haller GL; Sanchez-Sanchez M; Lercher JA, Impact of the local environment of Brønsted acid sites in ZSM-5 on the catalytic activity in n-pentane cracking. J. Catal 2014, 316, 93–102.

16. Li C; Vidal-Moya A; Miguel PJ; Dedecek J; Boronat M; Corma A, Selective Introduction of Acid Sites in Different Confined Positions in ZSM-5 and Its Catalytic Implications. ACS Catalysis 2018, 8 (8), 7688–7697.

17. Perea DE; Arslan I; Liu J; Ristanovic Z; Kovarik L; Arey BW; Lercher JA; Bare SR; Weckhuysen BM, Determining the location and nearest neighbours of aluminium in zeolites with atom probe tomography. Nat Commun 2015, 6.

18. Song C; Chu Y; Wang M; Shi H; Zhao L; Guo X; Yang W; Shen J; Xue N; Peng L; Ding W, Cooperativity of adjacent Brønsted acid sites in MFI zeolite channel leads to enhanced polarization and cracking of alkanes. J. Catal 2017, 349, 163–174.

19. Chen K; Abdolrahmani M; Horstmeier S; Pham TN; Nguyen VT; Zeets M; Wang B; Crossley S; White JL, Brønsted–Brønsted Synergies between Framework and Noncrystalline Protons in Zeolite H-ZSM-5. ACS Catalysis 2019, 9 (7), 6124–6136.

20. Gounder R; Jones AJ; Carr RT; Iglesia E, Solvation and acid strength effects on catalysis by faujasite zeolites. J. Catal 2012, 286, 214–223.

21. Gan Z; Hung I; Wang X; Paulino J; Wu G; Litvak IM; Gor'kov PL; Brey WW; Lendi P; Schiano JL; Bird MD; Dixon IR; Toth J; Boebinger GS; Cross TA, NMR spectroscopy up to 35.2T using a series-connected hybrid magnet. Journal of Magnetic Resonance 2017, 284, 125–136. [PubMed: 28890288]

22. Lafon O; Wang Q; Hu B; Vasconcelos F; Trébosc J; Cristol S; Deng F; Amoureux J-P, Indirect Detection via Spin-1/2 Nuclei in Solid State NMR Spectroscopy: Application to the Observation of Proximities between Protons and Quadrupolar Nuclei. The Journal of Physical Chemistry A 2009, 113 (46), 12864–12878. [PubMed: 19905016]

23. Trebosc J; Hu B; Amoureux JP; Gan Z Through-space R3-HETCOR experiments between spin-1/2 and half-integer quadrupolar nuclei in solid-state NMR. Journal of Magnetic Resonance 2007, 186, 220–227. [PubMed: 17379553]

24. Hu B; Trebosc J; Amoureux JP Comparison of several heteronuclear dipolar recoupling NMR methods to be used in MAS HMQC/HSQC. Journal of Magnetic Resonance 2008, 192, 112–122. [PubMed: 18299242]

25. Xue N; Vjunov A; Schallmoser S; Fulton JL; Sanchez-Sanchez M; Hu JZ; Mei D; Lercher JA, Hydrolysis of zeolite framework aluminum and its impact on acid catalyzed alkane reactions. J. Catal 2018, 365, 359–366.

26. Chen K; Kelsey J; White JL; Zhang L; Resasco D, Water Interactions in Zeolite Catalysts and Their Hydrophobically Modified Analogues. ACS Catalysis 2015, 5 (12), 7480–7487.

27. Motokura K; Matsunaga S; Noda H; Miyaji A; Baba T, Water-Accelerated Allylsilylation of Alkenes Using a Proton-Exchanged Montmorillonite Catalyst. ACS Catalysis 2012, 2 (9), 1942–1946.

28. Grey CP; Vega AJ, Determination of the Quadrupole Coupling Constant of the Invisible Aluminum Spins in Zeolite HY with 1H/27Al TRAPDOR NMR. J. Am. Chem. Soc 1995, 117 (31), 8232–8242.

29. Kentgens APM; Iuga D; Kalwei M; Koller H, Direct Observation of Brønsted Acidic Sites in Dehydrated Zeolite H-ZSM5 Using DFS-Enhanced 27Al MQMAS NMR Spectroscopy. J. Am. Chem. Soc 2001, 123 (12), 2925–2926. [PubMed: 11456997]

30. Wang Z; Jiang Y; Lafon O; Trébosc J; Duk Kim K; Stampfl C; Baiker A; Amoureux J-P; Huang J, Brønsted acid sites based on penta-coordinated aluminum species. Nature Communications 2016, 7, 13820.

31. Kerber RN; Kermagoret A; Callens E; Florian P; Massiot D; Lesage A; Copéret C; Delbecq F; Rozanska X; Sautet P, Nature and Structure of Aluminum Surface Sites Grafted on Silica from a Combination of High-Field Aluminum-27 Solid-State NMR Spectroscopy and First-Principles Calculations. J. Am. Chem. Soc 2012, 134 (15), 6767–6775. [PubMed: 22440230]

32. Lam E; Comas-Vives A; Copéret C, Role of Coordination Number, Geometry, and Local Disorder on 27Al NMR Chemical Shifts and Quadrupolar Coupling Constants: Case Study with Aluminosilicates. The Journal of Physical Chemistry C 2017, 121 (36), 19946–19957.
33. Wischert R; Florian P; Copéret C; Massiot D; Sautet P, Visibility of Al Surface Sites of γ-Alumina: A Combined Computational and Experimental Point of View. The Journal of Physical Chemistry C 2014, 118 (28), 15292–15299.
34. Engelhardt G & Michel D High-Resolution Solid-State NMR of Silicates and Zeolites (Wiley & Sons Austria, Limited, United States, 1987)
35. Hunger M, Multinuclear solid-state NMR studies of acidic and non-acidic hydroxyl protons in zeolites. Solid State Nucl. Magn. Reson 1996, 6 (1), 1–29. [PubMed: 8925262]
36. Frydman L; Harwood JS, Isotropic Spectra of Half-Integer Quadrupolar Spins from Bidimensional Magic-Angle Spinning NMR. J. Am. Chem. Soc 1995, 117 (19), 5367–5368.
37. Han OH; Kim C-S; Hong SB, Direct Evidence for the Nonrandom Nature of Al Substitution in Zeolite ZSM-5: An Investigation by 27Al MAS and MQ MAS NMR. Angew. Chem. Int. Ed 2002, 41 (3), 469–472.
38. Jiao J; Kanellopoulos J; Wang W; Ray SS; Foerster H; Freude D; Hunger M, Characterization of framework and extra-framework aluminum species in non-hydrated zeolites Y by 27Al spin-echo, high-speed MAS, and MQMAS NMR spectroscopy at B0 = 9.4 to 17.6 T. PCCP 2005, 7 (17), 3221–3226. [PubMed: 16240035]
39. Almutairi SM; Mezari B; Filonenko GA; Magusin PCM; Rigutto MS; Pidko E; Hensen EJM . Influence of Extraframework Aluminum on the Bronsted Acidity and Catalytic Reactivity of Faujasite Zeolite ChemCatChem 2013, 5, 452–466.
40. Abdolrahmani M; Chen K; White JL, Assessment, Control, and Impact of Brønsted Acid Site Heterogeneity in Zeolite HZSM-5. The Journal of Physical Chemistry C 2018, 122 (27), 15520–15528.
41. Nystrom S; Hoffman A; Hibbitts D, Tuning Brønsted Acid Strength by Altering Site Proximity in CHA Framework Zeolites. ACS Catalysis 2018, 7842–7860.
42. Li S; Zheng A; Su Y; Zhang H; Chen L; Yang J; Ye C; Deng F, Brønsted/Lewis Acid Synergy in Dealuminated HY Zeolite: A Combined Solid-State NMR and Theoretical Calculation Study. J. Am. Chem. Soc 2007, 129 (36), 11161–11171. [PubMed: 17705381]
43. Fritz PO; Lunsford JH, The effect of sodium poisoning on dealuminated Y-type zeolites. J. Catal 1989, 118 (1), 85–98.
44. Mota CJA; Bhering DL; Rosenbach N, A DFT Study of the Acidity of Ultrastable Y Zeolite: Where Is the Brønsted/Lewis Acid Synergism? Angew. Chem. Int. Ed 2004, 43 (23), 3050–3053.
45. Bhering DL; Ramírez-Solís A; Mota CJA, A Density Functional Theory Based Approach to Extraframework Aluminum Species in Zeolites. The Journal of Physical Chemistry B 2003, 107 (18), 4342–4347.
46. Ernst H; Freude D; Wolf I, Multinuclear solid-state NMR studies of Brønsted sites in zeolites. Chem. Phys. Lett 1993, 212 (6), 588–596.
47. Fyfe CA; Betherton JL; Lam LY Solid-State NMR Detection, Characterization, and Quantification of the Multiple Aluminum Environments in USY Catalysts by 27Al MAS and MQMAS Experiments J. Am. Chem. Soc 2001, 123, 5285–5291. [PubMed: 11457391]
48. Chen K; Gumidyala A; Abdolrhamani M; Villines C; Crossley S; White JL, Trace water amounts can increase benzene H/D exchange rates in an acidic zeolite. J. Catal 2017, 351, 130–135.
49. Silaghi M-C; Chizallet C; Sauer J; Raybaud P, Dealumination mechanisms of zeolites and extra-framework aluminum confinement. J. Catal 2016, 339 (Supplement C), 242–255.
50. Stanciakova K; Ensing B; Göltl F; Bulo RE; Weckhuysen BM, Cooperative Role of Water Molecules during the Initial Stage of Water-Induced Zeolite Dealumination. ACS Catalysis 2019, 9 (6), 5119–5135.
51. Pickard CJ; Mauri F, All-electron magnetic response with pseudopotentials: NMR chemical shifts. Physical Review B 2001, 63 (24), 245101.
52. Petrilli HM; Blöchl PE; Blaha P; Schwarz K, Electric-field-gradient calculations using the projector augmented wave method. Physical Review B 1998, 57 (23), 14690–14697.

53. Babitz SM; Williams BA; Miller JT; Snurr R; Haag W; Kung HH Monomolecular cracking of n-hexane on Y, MOR, and ZSM-5 zeolites. App. Catal. A: General 1999, 179, 71–86.

54. Ravi M; Sushkevich VL; van Bokhoven JA, Lewis Acidity Inherent to the Framework of Zeolite Mordenite. The Journal of Physical Chemistry C 2019, 123 (24), 15139–15144.

55. van Bokhoven JA; Koningsberger DC; Kunkeler P; van Bekkum H; Kentgens APM, Stepwise Dealumination of Zeolite Beta at Specific T-Sites Observed with 27Al MAS and 27Al MQ MAS NMR. J. Am. Chem. Soc 2000, 122 (51), 12842–12847.

56. van Bokhoven JA; Roest AL; Koningsberger DC; Miller JT; Nachtegaal GH; Kentgens APM, Changes in Structural and Electronic Properties of the Zeolite Framework Induced by Extraframework Al and La in H-USY and La(x)NaY: A 29Si and 27Al MAS NMR and 27Al MQ MAS NMR Study. The Journal of Physical Chemistry B 2000, 104 (29), 6743–6754.

57. van Bokhoven JA; van der Eerden AMJ; Koningsberger DC, Three-Coordinate Aluminum in Zeolites Observed with In situ X-ray Absorption Near-Edge Spectroscopy at the Al K-Edge: Flexibility of Aluminum Coordinations in Zeolites. J. Am. Chem. Soc 2003, 125 (24), 7435–7442. [PubMed: 12797818]

58. Janda J; Bell AT; Effects of Si/Al Ratio on the Distribution of Framework Al and on the Rates of Alkane Monomolecular Cracking and Dehydrogenation in H−MFI. J. Am. Chem. Soc 2013, 135, 19193–19207. [PubMed: 24237304]

59. Yang C; Janda A; Bell AT; Lin L, Atomistic Investigations of the Effects of Si/Al Ratio and Al Distribution on the Adsorption Selectivity of n-Alkanes in Brønsted-Acid Zeolites. J. Phys. Chem. C 2018, 122, 9397–9410.

60. Gounder R; Iglesia E The Catalytic Diversity of Zeolites: Confinement and Solvation Effects within Voids of Molecular Dimensions. Chem. Comm 2013, 49, 3491–3509. [PubMed: 23507832]

61. Gorte RJ; Crossley SP A Perspective on Catalysis in Solid Acids. J. Catal 2019, 375, 524–530.

62. Grossley SP; Resasco DE; Haller GL Clarifying the Multiple Roles of Confinement in Zeolites: From stabilization of transition states to modification of internal diffusion rates. J. Catal 2019, 372, 382–387.

63. To AT; Jentoft R; Alvarez WE; Crossley SP; Resasco DE Generation of Synergistic Sites by Thermal Treatment of HY Zeolite. Evidence from the Reaction of Hexane Isomers J. Catal 2014, 317, 11–21.

64. Zhang Y; Zhao R; Sanchez-Sanchez M; Haller GL; Hu J; Bermejo-Deval R; Liu Y; Lercher JA Promotion of Protolytic Pentane Conversion on H-MFI Zeolite by Proximity of Extra-framework Aluminum Oxide and Bronsted Acid Sites. J. Catal 2019, 370, 424–433.

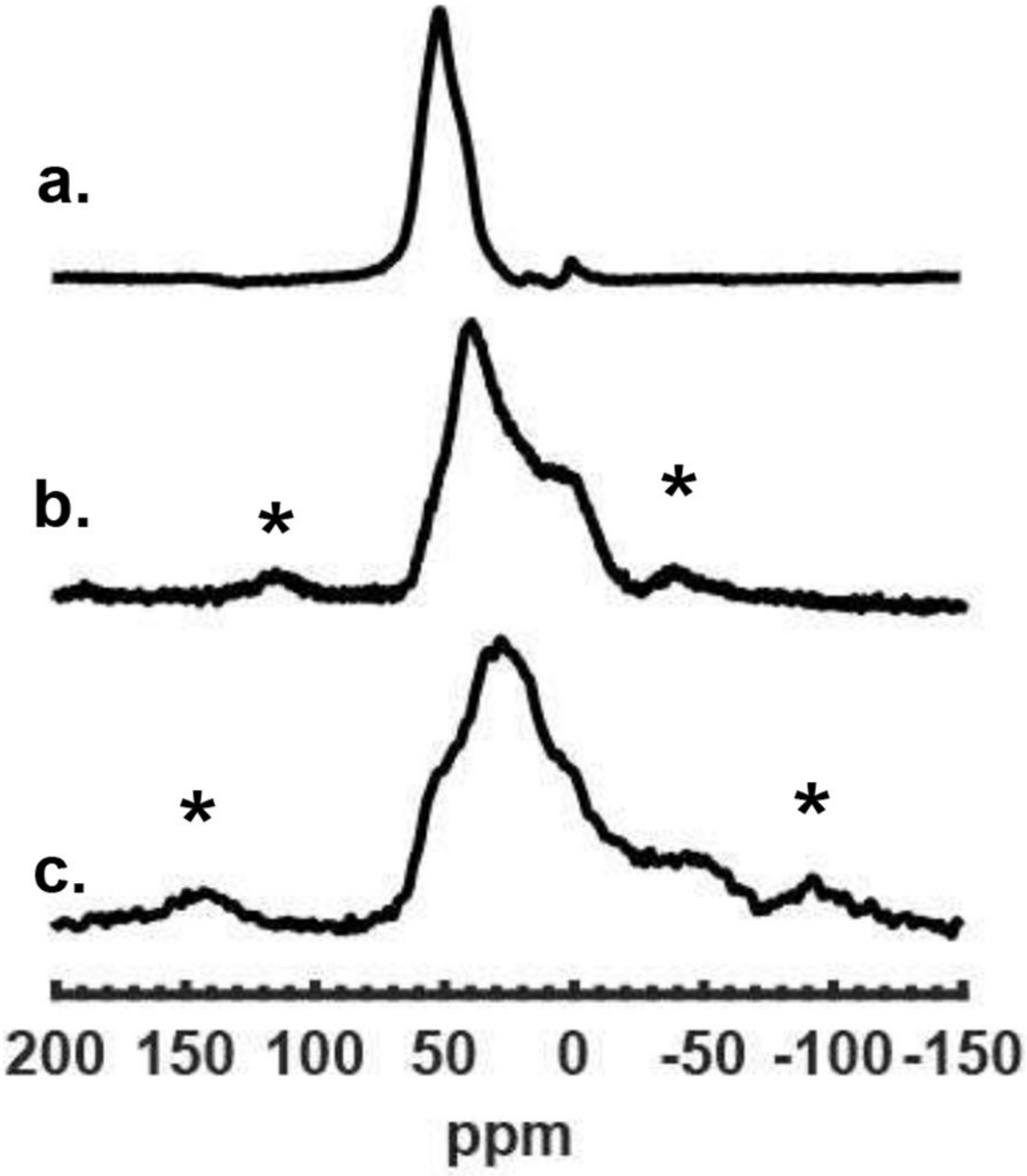

Figure 1.
^{27}Al MAS NMR spectra for dry HZSM-5 catalysts at (a) 35.2, (b) 19.6, and (c) 14 T magnetic field strengths. * denote spinning sidebands.

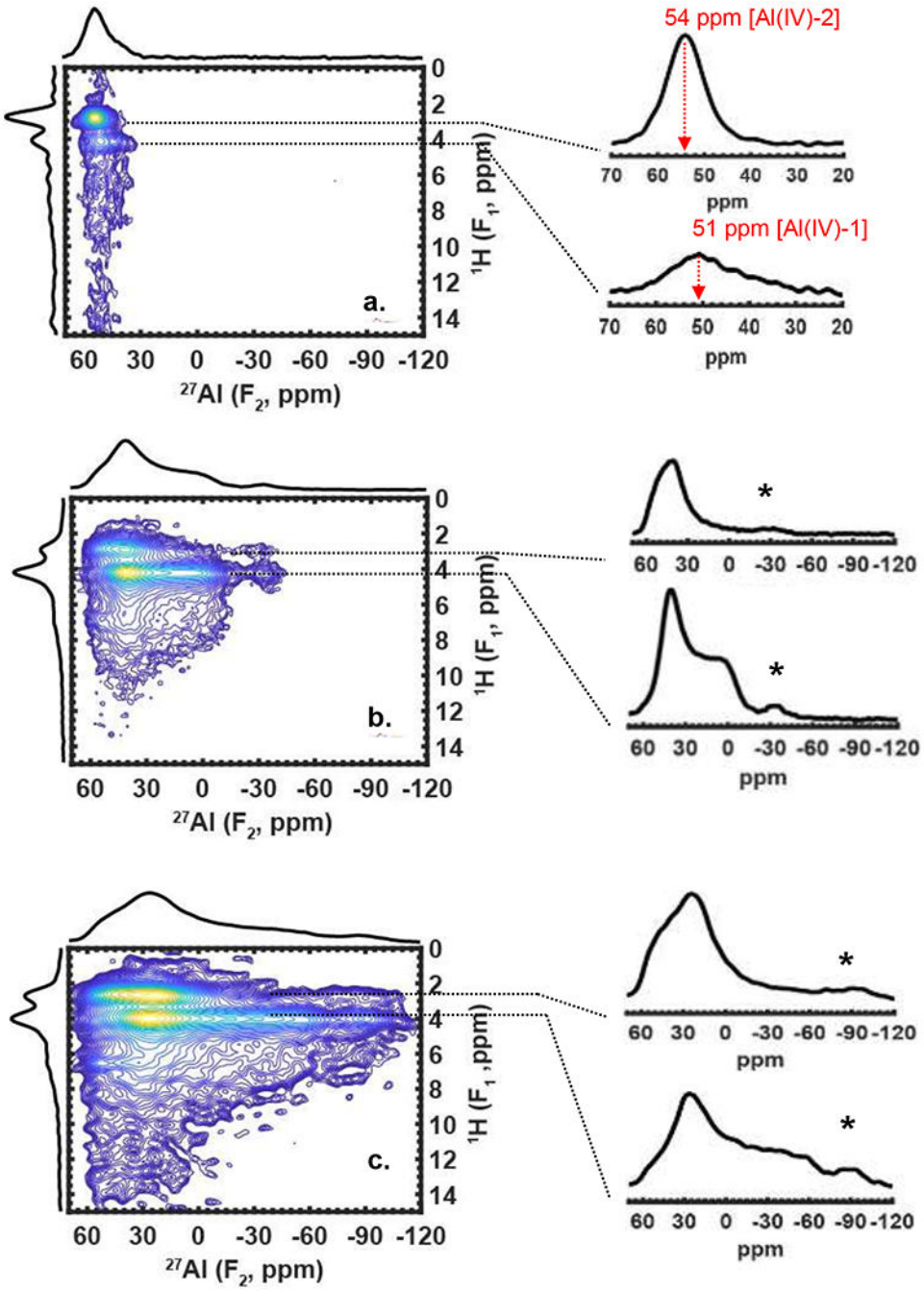

Figure 2.

^{27}Al{^{1}H} D-HMQC MAS NMR spectra for dehydrated HZSM-5 catalysts at **(a)** 35.2 T, **(b)** 19.6 T, and **(c)** 14.1 T. Slices are extracted from the ^{1}H dimension at 2.8 and 4.2 ppm, respectively, and are shown to the right of each contour plot. Note that the scale on the 35.2 T insets in (a) covers a much smaller chemical shift range than in (b) or (c). The data in (a) exclusively reveal the important spatial proximity based on dipolar couplings between the ^{27}Al spins and ^{1}H spins with chemical shifts at 54 ppm and 2.8 ppm, respectively. An

expanded view of the contour plot in (a) is provided in Figure S1 for convenience to the reader.

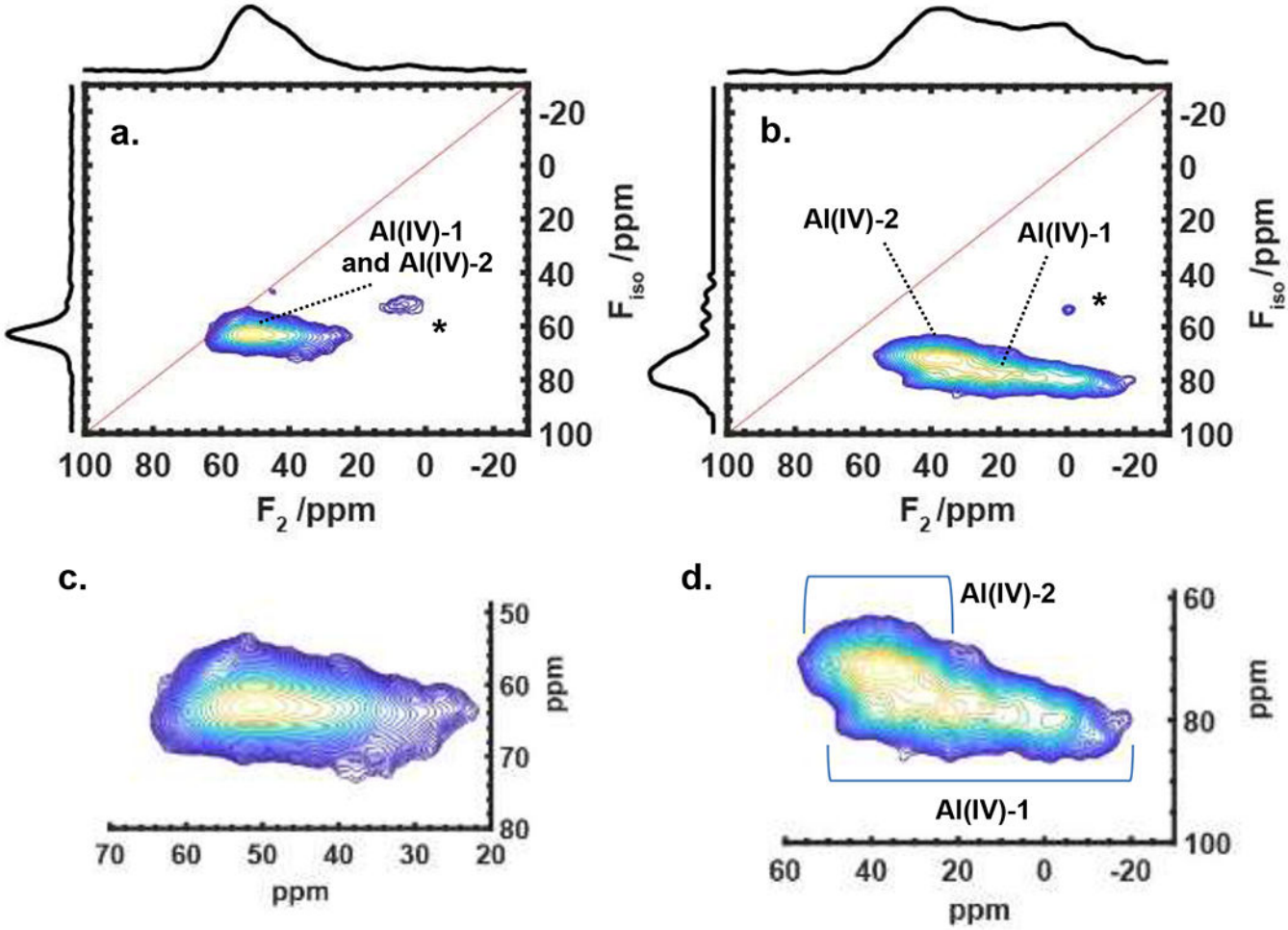

Figure 3.

^{27}Al triple-quantum MAS NMR results for dehydrated HZSM-5 catalysts at **(a)** 35.2 T and **(b)** 19.6 T, both acquired at 18 kHz MAS. The asterisks in (a) and (b) denote a folded first-order sideband, with some residual background contributing to the sideband intensity in (b). Expansions of the catalyst signal regions in (a) and (b) are shown in **(c)** and **(d)**, respectively. At 19.6 T, Al(IV)-1 and Al(IV)-2 are well resolved while at 35.2 T, both aluminum sites converge into one peak due to negligible δ_{qis}, further demonstrated in Figure S5. Notably, the Al(IV)-2 linewidth exceeds that of Al(IV)-1 in the isotropic F1 dimension, as also observed in the HMQC data. Spectra are plotted following the shearing transformation in F1.

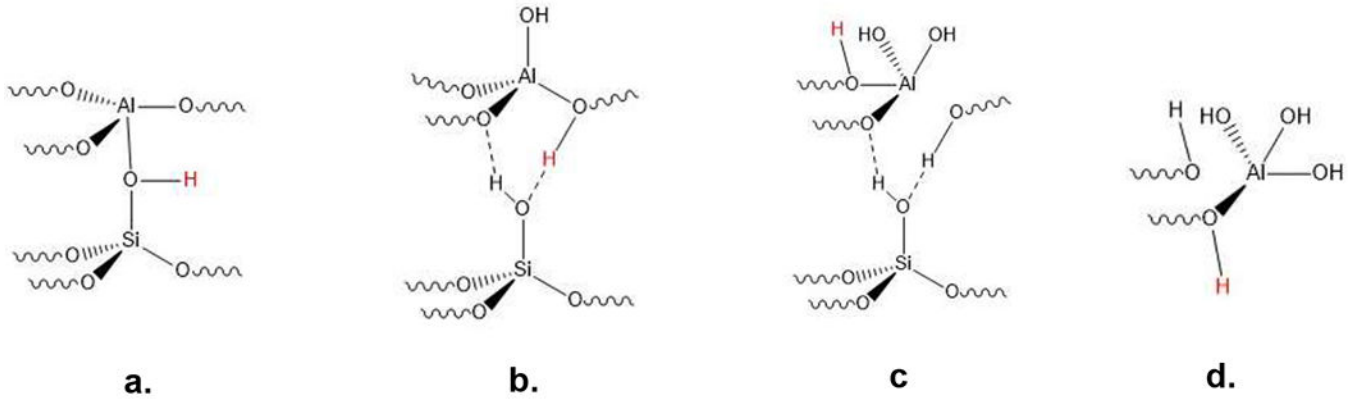

Figure 4.

Schematics depicting **(a)** the well-known BAS in the zeolite lattice, and intermediate structures formed via attack of **(b)** one, **(c)** two, and **(d)** three water molecules at the BAS. The Al atoms in structures (b) and (c) give rise to the Al(IV)-2 species.

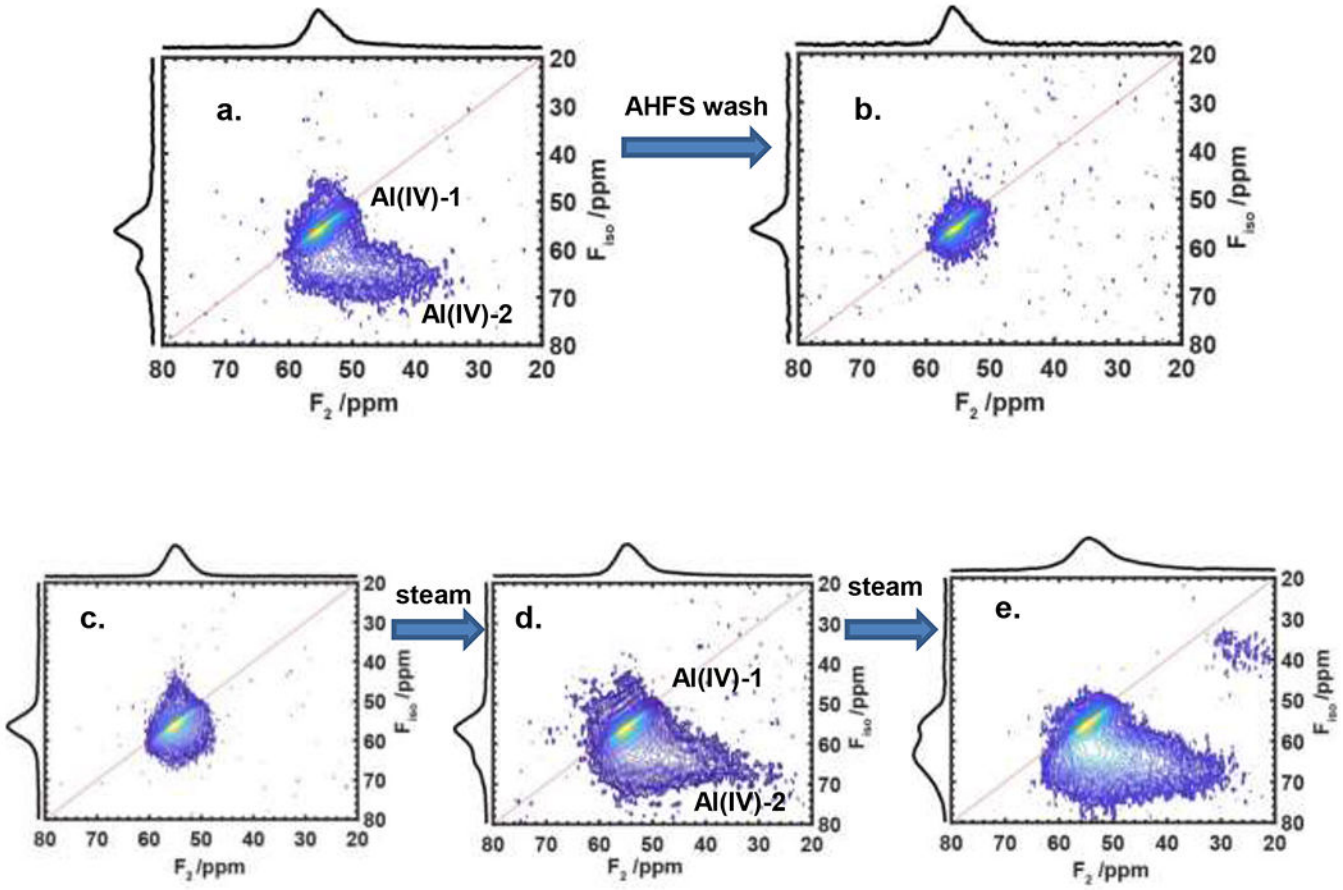

Figure 5.

^{27}Al triple-quantum MAS NMR results at 14 T for hydrated HZSM-5 catalysts as a function of post-synthetic treatments: **(a)** HZSM-5 with Si/Al=15; **(b)** same as in (a), following AHFS washing; **(c)** HZSM-5 with Si/Al=11.5; **(d)** same as in (c), following a mild steam treatment; **(e)** same as is in (c), following a severe steam treatment. Details of AHFS washing and steaming treatments are described in the SI. Figure S5 shows data for the sample in (a) obtained at four different magnetic field strengths under ambient hydration, demonstrating that the Al(IV)-2 signal cannot be an artifact nor can it arise from trivalent Al species.

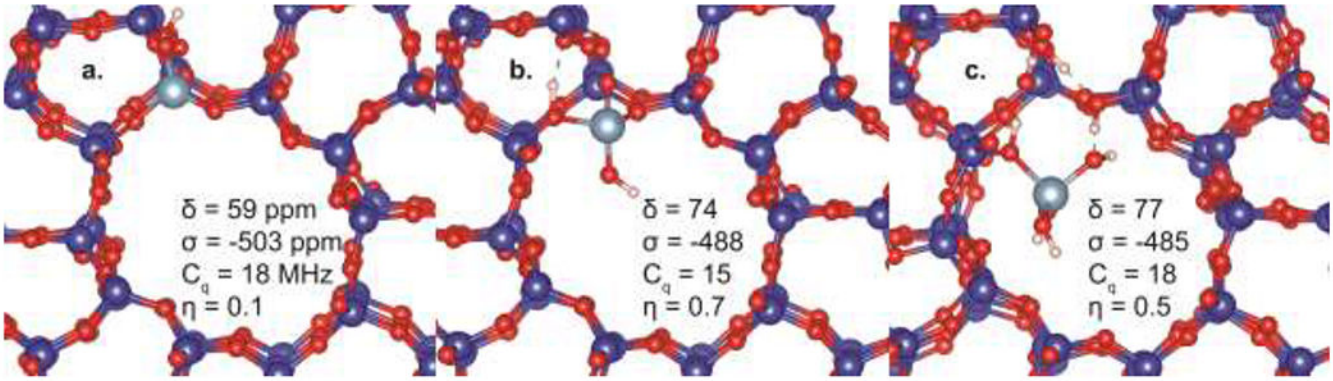

Figure 6.

Calculated DFT structures for **(a)** an isolated BAS containing only Al(IV)-1, and the partiallybonded Al(IV)-2 structure resulting from addition of **(b)** one water and **(c)** three waters to structure (a). Absolute chemical shielding values σ are in ppm units, quadrupole coupling constant Cq in MHz, and the asymmetry parameter η is unitless.

Table 1.

Quadrupolar and chemical shift parameters for the Al(IV)-1 and Al(IV)-2 sites determined via fitting of the single-pulse, HMQC, and MQMAS data in Figures 1–3 and in the Supplemental Information.

	Al(IV)-1	**Al(IV)-2**
Chemical shift distribution (ppm)	≤ 7	~ 8
P_q (MHz)	17	11
δ_{iso} (ppm)	55	59
η_Q	0.1	0.6

P_q = quadrupolar interaction product;

δ_{iso} = isotropic chemical shift value;

η_Q = quadrupole asymmetry parameter.

Table 2.

Comparison of conversion and reaction rate data as a function of Al(IV)-1 and Al(IV)-2 species, and their associated OH group concentrations:

Catalyst	Al(IV)-1 (mmol/g)[a]	4.2 ppm BAS OH signal (mmol/g)[b]	Al(IV)-2 (mmol/g)[b]	2.8 ppm OH signal (mmol/g)[b]	total Bronsted acidity (mmol/g)[c]	normalized n-hexane conversion per μmole Bronsted site[d]	Normalized H/D exchange rate constant for benzene reaction (s^{-1})[e]
Dry Si/Al=15	~ 0.67	0.56±0.018	~ 0.23	0.09±0.01	0.73	3%	23
Dry Si/Al=15 after AHFS wash	~ 0.60	0.54±0.020	~ 0.06	0.030±0.003	0.70	0.6%	1
Dry Si/ Al=11.5	-	0.61±0.02	-	0.05±0.01	1.08	1.3%	--

(a) from elemental analysis and quantitative 27Al NMR

(b) from quantitative 1H spin-counting NMR data;

(c) from IPA TPD measurements;

(d) from pulsed-microreactor data at 480°C with GC/MS detection;

(e) from room-temperature in-situ NMR of benzene-d6/HZSM-5 exchange reaction.